Experimental methods to determine inhalability and personal sampler performance for aerosols in ultra-low windspeed environments†

Darrah K. Schmees, Yi-Hsuan Wu and James H. Vincent*

Received 16th April 2008, Accepted 4th August 2008
First published as an Advance Article on the web 18th August 2008
DOI: 10.1039/b806431h

Most previous experiments of aerosol inhalability as it relates to particle aerodynamic diameter were conducted in wind tunnels for windspeeds greater than 0.5 m s^{-1}. While that body of work was used to establish an inhalable aerosol convention, results from studies in calm air chambers (for essentially zero windspeed) are being discussed as the basis of a modified criterion. Meanwhile, however, information is lacking for windspeeds in the intermediate range, which—it so happens—pertain to most actual workplaces. With this in mind, we have developed a new experimental system to assess inhalability and personal sampler performance for aerosols with particle aerodynamic diameter within the range from 6 to 90 μm for ultra-low windspeed environments from about 0.1 to 0.5 m s^{-1}. In this range of conditions for particle size and windspeed, controlled aerosol experiments are very difficult to perform, most notably with respect to the problem of achieving uniform spatial distributions of both test aerosols and air velocity. In the work reported in this paper, we have addressed these difficulties in a new, custom-designed experimental facility. It is a novel wind tunnel design that provides stable and controllable low-turbulence air movement, and allows for the delivery of test aerosol to the working section both from upstream (as in conventional wind tunnel experiments) and from above (as in calm air studies). In this system, losses by elutriation of particles that are being convected in the horizontal aerosol flow are compensated by particles entering from above by gravitational settling. An important feature of the new facility is the life-size, breathing mannequin that contains physical means to achieve any combination of mouth and nasal inspiration and expiration, and allows any desired relevant breathing flowrate and pattern by means of an external computer-controlled breathing simulator. Special steps were taken in the detailed design to ensure that particles may be collected during the inspiration phase of the breathing cycle and that the air during the expiration phase re-enters the breathing zone through a separate pathway (in order to avoid re-entrainment of collected particles). The mannequin itself was heated (to body temperature) to allow for the possibility that, at such low windspeeds, the overall air movement may be influenced by updrafts associated with the enhanced buoyancy of warm air near the body of the mannequin. The new experimental system has been commissioned and calibrated. Experiments have been carried out to determine the role of expired air and body heat on the time-dependent flow near the mannequin which might be expected to influence the transport, and hence inhalation, of particles. These show that such effects may be expected for some parts of the ranges of conditions studied. Preliminary experiments have been carried out to assess the aspiration efficiency of the human head. The successful development of this novel experimental facility paves the way for an important new series of experiments to evaluate inhalability under realistic workplace conditions, along with assessments of the performance of personal inhalable aerosol samplers.

Introduction

The physics governing the entry of airborne particles into the noses and mouths of human subjects during breathing are strongly dependent on a number of factors, primarily particle aerodynamic diameter,‡ windspeed and orientation of the subject with respect to the wind, as well as breathing flowrate and pattern. Similar factors are influential in how airborne particles are drawn into aerosol sampling devices. Thus the scientific link is established between actual human aerosol exposure and the technical sampling devices that are used to assess exposure. These scenarios have been discussed extensively in the literature.[1] The relationship between aerosol aspiration efficiency during inhalation and the other independent variables mentioned provide the basis of criteria by which to define what we have come to know as '*inhalability*'. An *inhalability criterion* therefore defines what might and what might not be inhaled, and to what degree, and so is the starting point for a scientific health-related standard. In turn, it also provides the yardstick for the performances of sampling instruments in a way that truly does reflect human exposure.

Department of Environmental Health Sciences, School of Public Health, University of Michigan, 109 S. Observatory, Ann Arbor, MI 48109-2029, USA. E-mail: jhv@umich.edu; Tel: +1 (734) 936-0703

† Presented at AIRMON 2008, January 28–31, 2008, Dr Holms Hotel, Geilo, Norway.

‡ Defined as diameter of an equivalent spherical particle of density 10^3 kg m^{-3} that has the same falling speed in air as the particle in question.

The development of health-related particle size-selective criteria for occupational aerosol sampling and standards is still of interest to standards-setting bodies, notably the International Standards Organization (ISO), the Comité Européen de Normalisation (CEN) and the American Conference of Governmental Industrial Hygienists (ACGIH).[2–4] Previous experiments to characterize inhalability and personal sampler performance—going back as far as the late 1970s and continuing into the 1990s—were mostly carried out in wind tunnels with windspeeds in excess of 0.5 m s^{-1}. These were all based on the experimental determination of *aspiration efficiency* (A) for life-sized, breathing mannequins with orientation with respect to the wind averaged over all possible orientations. From the results, an inhalability convention was proposed, and widely adopted by bodies like those mentioned above, taking the form

$$I(d_{ae}) = 0.5\{1 + \exp(-0.06d_{ae})\} \quad (1)$$

where I is *inhalability* itself and d_{ae} is particle aerodynamic diameter [expressed in μm], and is based on the experimental measurements that were reported for A. This expression is now widely referred to as the *CEN/ISO/ACGIH inhalability criterion* and applies for the range of d_{ae} up to 100 μm, beyond which it is acknowledged that no data exist on which to base such a curve (although noting that this does not represent a cut-off). The form of I as expressed in eqn (1) currently underpins many regulatory standards for workplace aerosols around the world. However, studies in modern industrial workplaces indicate that, in reality, average windspeeds are much lower even than the bottom end of the range covered by the original inhalability experiments, and are typically between 0.05 and 0.25 m s^{-1}.[5,6] Therefore, the current CEN/ISO/ACGIH convention may not be entirely appropriate. Some work has been reported where aspiration efficiency of the human head was determined in calm air,[7] but this does not shed much light on how aspiration efficiency behaves in the important intermediate low-windspeed range of interest. A knowledge gap is therefore identified.

With the preceding in mind, a new experimental program was initiated to determine the aspiration efficiency of the human head in this low-windspeed range, and—in due course—to characterize the corresponding performances of personal aerosol samplers. It was known at the outset that studies in the range of conditions indicated would present some very considerable difficulties (which perhaps explains why such experiments have not been carried out previously), and so would require special experimental considerations. So the main thrust of this paper is to describe the new experimental arrangements that we have developed. It describes the rationale for the new work, the design and construction of the new facilities, and some preliminary results, pointing the way forward towards the acquisition of aspiration efficiency data that will enable the inhalability criterion to be revised (where appropriate) to make it more relevant to real world conditions. More comprehensive data for this purpose are already being acquired and will be reported separately.

Rationale

The rationale for the new research begins with identifying the key features of the faster moving air scenario on the one hand and calm air on the other. At issue are the relative magnitudes of the velocity of the horizontally-moving air and the velocity with which the particles fall under gravity. It is useful to note, for example, that the falling speed of a particle with d_{ae} = 30 μm is about 0.03 m s^{-1}, with d_{ae} = 60 μm is 0.10 m s^{-1} and with d_{ae} = 80 μm is 0.17 m s^{-1}.[8] So, in the wind tunnel experiments upon which the original inhalability criterion was based, the trajectories of the particles for most of the particle size range of interest would have been almost horizontal, such that it was the moving external air that was primarily responsible for bringing the particles into the breathing zone of the mannequin (by convection). By contrast, in calm air, gravitational settling is the sole means by which particles are brought into the breathing zone. It is therefore seen that the physical scenarios for the two contrasting scenarios are very different, as it is for aerosol sampling in general.[1] Importantly, in the intermediate regime, both mechanisms feature significantly together, to a greater or lesser extent depending on both windspeed and particle size. This is the source of the considerable experimental difficulties that are addressed in this paper.

The challenge is to develop an experimental arrangement in which sufficiently uniform aerosol distribution may be achieved in a test system in order that valid measurements of aspiration efficiency for the human head—leading to inhalability—may be carried out. This was achieved by means of what might best be described as a 'hybrid' ultralow-windspeed facility, combining elements of both a wind tunnel and a calm air chamber. It is shown in its most idealized form in Fig. 1. Fig. 1a identifies the main features, indicating in particular the provision to introduce

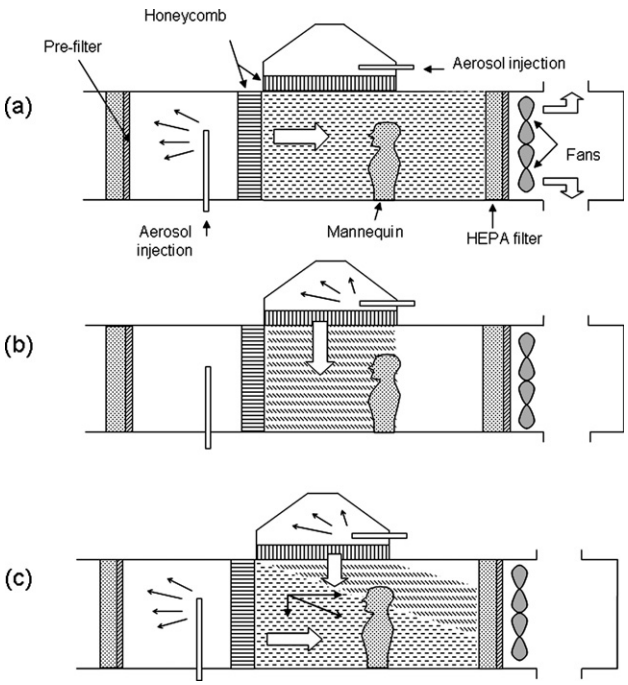

Fig. 1 Schematics to show the concept of the new ultralow-speed wind tunnel: (a) the higher windspeed situation where particle settling velocity is relatively negligible; (b) the calm air situation where all the airborne particles in the test section arrive there vertically by gravitational settling; and (c) the ultralow-windspeed situation where aerosol in the test section receives contributions from both upstream and above.

test aerosol from upstream (as in a wind tunnel) and from above (as in a calm air chamber). In principle, each aerosol injection location may be adjusted with respect to the other to provide uniform spatial distribution of the aerosol in the working section. In particular, Fig. 1a illustrates the higher windspeed situation where particle settling velocity is negligible, so that all the airborne particles in the test section arrive there by horizontal convection. Fig. 1b illustrates the calm air situation where all the airborne particles in the test section arrive there vertically by gravitational settling. Fig. 1c is the most interesting in the context of the current work, showing how aerosol in the test section receives contributions from both upstream and above. It indicates the horizontal and vertical velocity vectors for particles of a given size, revealing the non-horizontal resultant trajectory. For the idealized system shown, particles from upstream falling out of the test section by gravity are compensated by particles from above arriving there by gravity. So in principle it should be possible to maintain both uniform spatial distribution of concentration and particle size distribution. It remained to be seen how this applies in reality.

As already mentioned, the primary index of interest, and hence the subject of measurement, is the *aspiration efficiency* of the human head (as represented by a life-sized mannequin, inert but with simulated breathing and body heat) and—eventually—of personal samplers mounted on the body of the torso. In general, aspiration efficiency for the entry of airborne particles into an opening into which air is being drawn is defined as the ratio of the concentration of the aerosol entering through the plane of the opening and that in the undisturbed air sufficiently distant from the opening as to be undisturbed by its presence and action. The latter metric of concentration is commonly referred to as the '*reference concentration*'. For air that is moving, no matter how slowly, this is defined in terms of an upwind location in the freestream.

Physical interpretation of measurements of the aspiration efficiency of the human head and the personal samplers of interest is inevitably linked with the character of the air flow around the body. This is complicated, influenced in the first instance by the nature of the freestream (*e.g.*, intensity and scale of turbulence) and then by the cyclical time-varying influence of the inspiration and expiration of air by the mannequin. For the latter, the expiration phase is the most interesting because it involves a time-varying jet that is projected into—and mixes with—the freestream. There are elegant experimental methods that may be applied to examine these phenomena, including instrumentation (*e.g.*, laser Doppler anemometry) that can allow mapping of the flow field in great detail. In addition there are modern computer fluid dynamic (CFD) procedures that can be applied successfully to flows even as complex as the one near the mannequin.[9] However, these are less immediately instructive. An alternative qualitative approach is flow visualization, in which a visible tracer is introduced into the airflow upstream of the mannequin, and its appearance recorded either by the naked eye or by some photographic imaging process. Appropriate flow visualization of the complex time-varying flow around a heated, breathing mannequin can shed important qualitative light on the nature of the flow, and provide a basis for interpretation of the aerosol transport that underpins aspiration efficiency.

Experimental set-up and methods

Ultralow-speed wind tunnel

A new wind tunnel was developed on the basis of considerations like those described above. For this we worked with Engineering Laboratory Design (Lake City, MN, USA) who had built previous aerosol test facilities for our group. It was designed to be capable of: (a) containing a life-sized human mannequin, including the full torso above the waist; (b) providing uniform, smooth air flow at velocities continuously variable between 0.05 and 0.50 m s^{-1}; and (c) enabling the injection of spatially-uniform test aerosols (along the lines already indicated) with well-defined particle size distributions for mass median aerodynamic diameter (MMAD) in the range up to about 100 μm. The fully-realized facility measured 1.22 m × 1.22 m in cross-section and approximately 6 m in overall length, with the actual working section for aerosol sampling measuring 3 m in length. Air entered the system through a pre-filter, passing through an upstream mixing chamber, and then—in the original version—passing through a metal honeycomb screen that served to straighten the air flow entering the working section and minimize the penetration of turbulent motions, in particular those derived from the upstream aerosol injection. The air flow itself was generated by four downstream fans, the speeds of which were regulated and synchronized by means of a frequency inverter, enabling easy manipulation of the windspeed. Finally, the air was discharged back into the laboratory through a system of pre- and HEPA filters located just in front of the fans. A photograph of the new ultralow-windspeed facility is shown in Fig. 2.

Windspeed measurement by anemometry at such low air velocities is very difficult. Most conventional instruments—hot-wire or pitot-static tubes, for example—are not usable. So, for our experiments, we developed a homemade 'time-of-flight' method. Here, a stream of smoke was released into the wind tunnel in the upstream section ahead of the honeycomb section (fuller details are given below), and a 'blip' was introduced by tapping on the tube through which the smoke entered the tunnel. At such low windspeeds, such blips remained coherent and so were very easy to track using the naked eye as they traveled downstream. By visually tracking each blip as it traveled downstream, and timing it with a stop-watch as it passed between a pair of marker points a known distance apart, it was a very simple—and very accurate—matter to determine the windspeed in the range of interest. The freestream air velocity measured in this way was shown to be sufficiently uniform throughout the

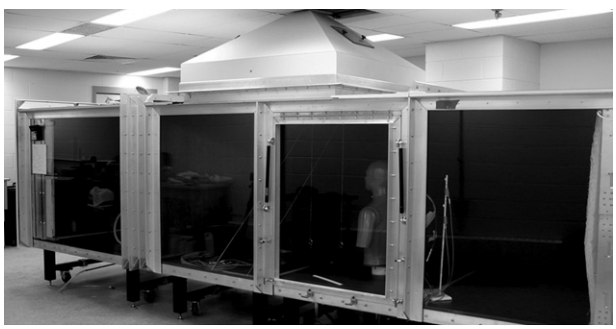

Fig. 2 Photograph of the ultralow-speed wind tunnel.

windtunnel, and was subsequently calibrated against the pressure drop across the large air filter at the entrance to the wind tunnel, as measured using a micromanometer. The resultant graph of pressure drop *versus* actual windspeed provided quick and accurate windspeed measurement on a day-to-day basis. Of course, the pressure drop characteristics of the filter could be expected to change over time as particles from the laboratory were collected on the filter media. So the calibration was checked on a regular basis.

Test aerosol

The aerosols used for these, and all subsequent experiments, were generated from narrowly graded powders of fused alumina (*Duralum*, Washington Mills, Niagara, NY, USA), similar to those used previously in our laboratory and elsewhere and initially characterized in 1985 by Mark *et al.*[10] A range of powder grades was chosen in order to generate aerosol covering the wide range of particle sizes of interest, including F1200, F800, F500, F400, F280 and F240, known from long experience to consistently generate aerosols with nominal particle aerodynamic diameters of 6 μm, 13 μm, 26 μm, 34 μm, 74 μm, and 89.5 μm, respectively, when delivered into wind tunnels, and with low geometric standard deviations (generally less than 1.30). These powders were aerosolized using a mechanical dust generator (Topas SAG 410, Dresden, Germany) and injected into either the top mixing cone, the upstream mixing chamber or in both simultaneously, depending on the particle size and windspeed of interest. Prior to their use, in order to reduce inter-particle adhesion and hence ensure optimum dispersion, powder samples were conditioned overnight in an oven. Then during the experiments themselves, the powder contained in the feed hopper of each generator was subject to radiant heat from an infrared lamp, in order to maintain the desired low moisture content. The pressure of the air delivered to the aspirator of each generator was maintained above 2 bar, high enough to break up any agglomerates during aerosolization from the bulk powder.[11] No electrical neutralization was performed in the light of the well known fact that aerosol particle charge has insignificant effect on aspiration efficiency.[1]

Aerosol delivery

Development of the details of the aerosol delivery systems, both upstream and above, required special regard to the difficulties involved in obtaining sufficient mixing of the aerosol prior to its delivery to the working section, leading to the optimum uniformity of test aerosol within the working section. Such difficulties were well known to be magnified at low windspeeds like those of interest in this work.

For the aerosol generation from upstream, a dual tracking system was developed (see Fig. 3). Here, the injection nozzle was mounted on a motor that allowed for the nozzle to be moved vertically in a reciprocating motion such that, during a given cycle, the aerosol could be delivered alternately between the upper and the lower parts of the working section. The reciprocating motor in turn was mounted on an overhead tracking system that conveyed it laterally backwards and forwards across the width of the entrance to the working section. The nozzle itself

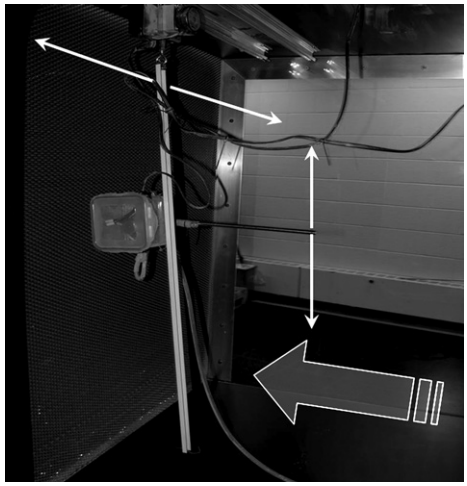

Fig. 3 Photograph of the upstream aerosol delivery system, indicating the tracking systems by which to achieve uniform dispersal into the working section. The large arrow indicates the direction of air movement.

was placed such that the aerosol was injected in the general upstream direction, thus ensuring improved spatial distribution as it blew back over the injection system. By means of this complex system of moving components, the aim was to generate a spatial distribution of the test aerosol in the working section that was uniform *when averaged over time*. This system we have described is similar in principle to that described by Hinds and Kuo for their own mannequin studies.[12] For the aerosol generation from above, a similar oscillating system was employed in the upper mixing section in order to provide uniform delivery—again when averaged over time —of aerosol to the top of the working section. Both delivery systems were adjusted by trial and error to arrive at the optimum placements for uniform test aerosol concentration.

Preliminary trials with this experimental system soon revealed some important features that represented departures from the simple idealizing assumptions implicit in the original rationale discussed earlier. In the first instance, it was found that aerosols representing the coarsest powder grades were not significantly present in the working section (notably F400, F280 and F240, even at the higher end of the windspeed range used). It was clearly apparent that this was due to the fact that the largest particles were collected efficiently by elutriation inside the individual tube-like elements of the honeycomb section located immediately upstream of the working section. Similarly, for aerosols generated from all powders delivered from above at the higher end of the windspeed range used, it was not possible to obtain the desired uniform spatial distribution due to the large entry angle of aerosols into the wind tunnel working section from above. So it was concluded that, for the initial lay-out of the experimental system, only a limited part of the overall range of desired experimental conditions could be examined: namely, finer grades delivered from upstream and coarse grades delivered from above only at the lowest windspeeds. To overcome the limitations for the coarser aerosols, wind tunnel modifications were made. Most notably, the metal honeycomb section located at the entrance to the working section was replaced by a pair of aluminium perforated plates, with circular openings 4 mm in

Table 1 Dust generator (Topas SAG 410) settings for all combinations of windspeed and powder grade, as indicated by the percentage of the belt speed for the contribution of aerosols from both upstream and overhead

	Windspeed/m s^{-1}					
	0.10		0.24		0.42	
Powder grade	Upstream (%)	Overhead (%)	Upstream (%)	Overhead (%)	Upstream (%)	Overhead (%)
F1200	25	25	25	0	25	0
F800	25	25	25	0	25	0
F500	25	5	25	0	25	0
F400	25	5	25	0	25	0
F280	0	10	50	5	25	5
F240	0	10	50	5	40	5

diameter on 60° centers and with open area 63%. The dimensions were chosen to minimize the downstream propagation of free-stream turbulence, but now with minimal particle losses by inertial deposition and none of the previous elutriation losses. The new set-up now enabled experiments to be performed at all windspeeds for all powders of interest. However, the nature of the air flow in the working section was essentially quite similar to that of the original set-up.

Optimal settings for the two aerosol generators—for horizontal and vertical aerosol delivery, respectively—were determined, again by trial and error, in order to achieve the most uniform aerosol concentration in the wind tunnel working section across the ranges of conditions of interest. These are summarized in Table 1, where the percentages indicated relate to the belt speed settings of the particular types of generators used (*i.e.*, the Topas SAG 410).

Characterization of the test aerosol

For all the aerosols generated and dispersed into the new ultralow-windspeed wind tunnel, the first step in their characterization was to identify two planes in the working section. The first was the one representing the location of the mannequin (the *mannequin plane*); the second was the one representing the location of the reference sampler 0.75 m upwind of the mannequin plane (the *reference plane*).

From the outset, it was expected that a major challenge for this novel experimental system would derive from the fact that, at such low windspeeds, it would be difficult to achieve spatial uniformity of the test aerosol in the working section. In addition, it was expected that there would be particle losses during dispersal and delivery to the working section such that the particle size distribution would be modified (as compared to that for the originally-generated test aerosol). With this in mind, experiments were conducted to answer three specific questions:

(1) To what extent is the aerosol concentration uniform throughout both the reference and the mannequin planes for each aerosol and for each windspeed?

(2) What is the ratio of the average concentrations in the reference and mannequin planes?

(3) What are the mass median aerodynamic diameter (MMAD) and the geometric standard deviation (σ_g) at the mannequin plane for each set of experimental conditions?

The experiments to answer these questions were in fact calibrations and therefore represented an important characterization of the experimental system.

Aerosol concentration. To answer the first two questions, local measurements of aerosol concentration at both the reference and the mannequin planes were performed using IOM personal inhalable samplers (SKC Inc, Eighty-Four, PA, USA), used facing directly upwards as *static samplers*. The selection of this particular sampler for static aerosol concentration measurements was arbitrary and based on practical considerations, including employment of the stainless steel cassette which enabled easy gravimetric analysis with minimal sample losses and moisture uptake, along with knowledge from extensive experiments reported elsewhere that it efficiently collects particles over the full range of particle sizes of current interest. Since the primary objective of this particular set of the experiments was to determine the spatial uniformity of the concentration throughout the wind tunnel, the choice of this sampler and its mode of use were considered satisfactory. For the experiments described here, the mannequin was removed from the wind tunnel and three to five IOM samplers were located at points covering the top, center and bottom of each plane, with the majority of experiments performed for the corners and center of a structure like the one shown below in Fig. 4. In this way, the four outer samplers occupied positions representing the centroids of the four quadrants, and the fifth sampler at a location representative of the position of the mannequin (when in place). For experiments utilizing three sampling points, these represented the top, center and bottom points along the central vertical axis of the wind tunnel. As indicated, initial experiments were performed for three different powder grades (F1200, F800 and F500) and three different windspeeds (0.10 m s^{-1}, 0.24 m s^{-1} and 0.42 m s^{-1}), thus covering a total of nine conditions of interest. After the wind

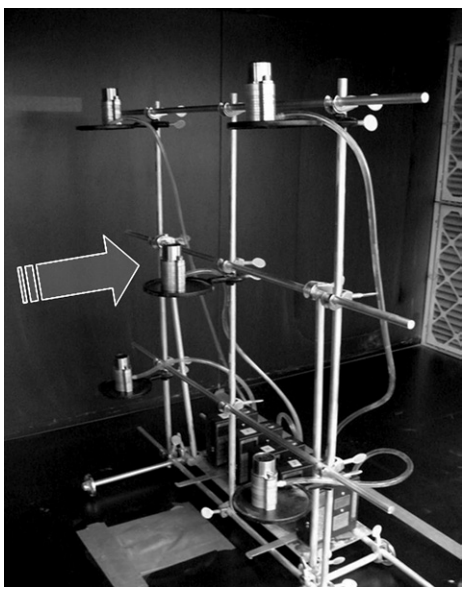

Fig. 4 Photograph of the system by which to measure aerosol particle size distribution and concentration at locations over the working cross-section of the ultralow-speed wind tunnel, showing the five modified Marple cascade impactors.

Table 2 Uniformity of aerosol concentration along the vertical axis of the windtunnel, across both sampling planes, shown as the average ratio of individual sampling points to the center point, listed with standard error, and values indicated that are statistically different from the center point

		Top		Bottom	
Powder grade	Windspeed/m s^{-1}	Ratio	SE	Ratio	SE
F1200	0.10	1.08	0.08	0.71[a]	0.01
	0.24	1.28	0.32	0.78	0.23
	0.42	0.65[a]	0.04	0.59[a]	0.03
F800	0.10	0.96	0.05	0.81[a]	0.05
	0.24	1.03	0.04	0.72	0.08
	0.42	0.68[a]	0.02	0.61[a]	0.03
F500	0.10	0.78	0.01	0.68	0.35
	0.24	0.99	0.06	0.82	0.01
	0.42	0.83	0.06	0.80	0.03
F400	0.10	0.87	0.27	1.00	0.10
	0.24	0.72[a]	0.09	0.72[a]	0.05
	0.42	1.47	0.55	1.48	0.49
F280	0.10	1.08	0.68	0.91	0.46
	0.24	0.98	0.01	1.03	0.27
	0.42	0.94	0.48	1.04	0.18
F240	0.10	1.01	0.34	1.16	0.14
	0.24	1.04	0.40	1.31	0.07
	0.42	0.67	0.03	1.13	0.45

[a] Difference from center is statistically significant at $\alpha = 0.05$.

tunnel modification, the uniformity of aerosol concentration for all six powder grades of interest at all three windspeeds, representing 18 experimental conditions, was again assessed in this way. The results were analysed in order to assess the overall variability of the concentration within the sampling planes (*i.e.*, differences along the vertical axes of the wind tunnel working section, as well as the average difference between the upstream reference and downstream mannequin planes). Table 2 summarizes the vertical variability, expressed as the relative concentrations for the top and bottom portions of the wind tunnel working section with respect to the center location, along both planes collectively. These results indicate that, while concentrations were fairly uniform, there are several conditions for which the outer sampling points showed statistical differences in measured concentration. Typically these differences were seen at the highest windspeeds for the smallest particles. In the cases where both the top and bottom had significantly different concentrations relative to the center, these differences may have been artifacts associated with the upstream aerosol injection system and the limitations of its range of spatial dispersion (*i.e.*, at higher windspeeds, we noticed a tendency for particles to stay closer to the center portion of the wind tunnel). Table 3 summarizes the ratios of the aerosol concentration between the reference and mannequin planes. The results indicate that the differences were less than about 10%, statistically significant only for the largest particles sizes.

Finally, Table 4 summarizes the ratios for aerosol concentration between each plane, this time measured on the wind tunnel center line using the thin-walled cylindrical sampling probes that were used for the actual reference sampling in the experiments that were the primary objective of this work. It is these ratios that were used as the correction factors, to be applied to the reference sampler concentrations to estimate the actual aerosol concentration to which the mannequin was exposed in those experiments.

Table 3 Uniformity between reference and mannequin planes, as represented by the average ratio of measurements for each sampling point on each plane for all powder grades and windspeeds of interest, based on three measurements for each plane, with standard error given

	Windspeed/m s^{-1}					
	0.10		0.24		0.42	
Powder grade	Ratio	SE	Ratio	SE	Ratio	SE
F1200	1.03	0.05	0.95	0.16	0.96	0.04
F800	1.02	0.04	1.06	0.10	0.97	0.05
F500	0.89	0.26	0.93	0.04	0.87	0.04
F400	0.89	0.20	1.08	0.09	0.71[a]	0.11
F280	2.50	1.66	0.67[a]	0.13	0.87	0.30
F240	6.95[a]	2.33	1.22	0.34	1.00	0.33

[a] Difference between reference and mannequin plane is statistically significant at $\alpha = 0.05$.

Table 4 Correction factors to be applied to the reference sampler measurement of aerosol concentration for the determination of the actual aerosol concentration at the mannequin plane for calculating the aspiration efficiency of the mannequin head, as measured by the ratio of the center point concentration on each plane, shown with the standard error

	Windspeed/m s^{-1}					
	0.10		0.24		0.42	
Powder grade	Ratio	SE	Ratio	SE	Ratio	SE
F1200	1.04	0.06	1.07	0.02	0.98	0.08
F800	1.03	0.11	1.06	0.02	1.06	0.02
F500	1.26	0.02	1.00	0.01	1.15	0.04
F400	1.19	0.04	0.80	0.03	0.98	0.17
F280	0.94	0.07	0.71	0.05	1.22	0.08
F240	2.90	0.73	0.65	0.06	0.78	0.01

Aerosol particle size distribution. Based on considerations along the lines already described, it was reasonable to expect that—in the ultralow-windspeed environment in the new facility—particle size distributions might have been significantly modified during dispersal into the tunnel and conveyance into the working section. So it was important to assess the particle size distribution of the test aerosol in the working section and to examine the extent to which the mass median aerodynamic diameter (MMAD) and geometric standard deviation (σ_g) for aerosols generated from each powder grade differed from the nominal values reported previously. We therefore measured the particle size distribution for each of the full set of experimental conditions already identified. Only for the test aerosol derived from the coarsest-grade particles delivered only from the upper chamber (namely, powder grades F280 and F240 for 0.10 m s^{-1} only) was it assumed that there were no significant loses during entry downwards into the test section—in which cases the original, nominal particle size distribution was considered appropriate. The particle size distribution was measured at both the center of the reference and mannequin planes concurrently, with

Table 5 Particle size distributions for all powder grades and windspeeds of interest in the fully modified wind tunnel set-up, as represented by mass median aerodynamic diameter (MMAD) and geometric standard deviation (σ_g)

	Windspeed/m s^{-1}							
	0.10		0.24		0.42		Nominal size	
Powder grade	MMAD	σ_g	MMAD	σ_g	MMAD	σ_g	MMAD	σ_g
F1200	9.6	1.28	9.5	1.32	9.3	1.34	6.0	1.36
F800	13.9	1.49	12.8	1.47	12.4	1.56	13.0	1.38
F500	28.8	1.62	32.7	1.71	28.7	1.93	26.0	1.30
F400	37.7	1.62	44.3	1.59	40.0	1.74	34.0	1.20
F280	74.0[a]	1.19[a]	62.4	1.42	66.9	1.45	74.0	1.19
F240	89.5[a]	1.29[a]	60.1	1.45	63.0	1.49	89.5	1.29

[a] Nominal value used for this condition.

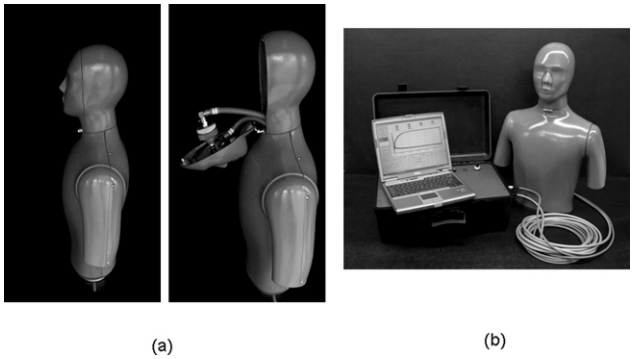

Fig. 5 Photographs of the mannequin: (a) both assembled and disassembled (face manifold dropped down) to reveal aerosol collection filter and internal connections; and (b) the mannequin system, including the breathing machine and control laptop computer.

two repeats for each set of conditions. The measurements were performed using versions of the Marple personal cascade impactor (Model 290, from SKC Inc., Eighty Four, PA, USA) that had been modified with an additional, porous plastic foam top stage to extend the upper end of the sampler's useful particle size range.[13] Table 5 summarizes the particle size distributions that were obtained by averaging the data from all samplers over all tests. The averaging was achieved by combining the mass ratio collected at each impactor stage for all samplers, and plugging them into a simple inversion algorithm, modified only by correcting the aspiration efficiency of the instrument for the low windspeeds pertaining to the present scenario. The results in Table 5 indicate that the particle size distributions for the given powder grades, except for powder F800, were indeed significantly different from the nominal ones. In addition, σ_g was generally greater than the original, nominal ones.

The values given in Table 5 were the ones that were used to define the test aerosol for the various sets of conditions pertaining to the primary experiments that are described below (and more that will feature in future reports of this work).

Heated, breathing mannequin

The measurement of aspiration efficiency of the human head required a suitable model to simulate the relevant aspects of the human respiratory system, most notably the ability to simulate the external movement of air into the nose and mouth of a human subject. To achieve this, we worked in cooperation with Measurement Technology Northwest, Seattle, WA, USA, who had previously built heated, breathing mannequins for other applications. The goal was to: (a) realize a life-size mannequin with accurately modeled external human features; (b) simulate continuously-variable, representative breathing rates; (c) allow for inspiration and expiration through either the nose or mouth, in any combination; (d) enable collection of all inhaled particles; (e) provide a representative range of body temperatures; and (f) fit into the new wind tunnel with the ability to rotate continuously about a vertical axis through a full 360°. The resultant system is shown in the photographs in Fig. 5. Fig. 5a shows the mannequin itself, on the left-hand side fully assembled and on the right-hand side with the face-piece dropped down to reveal the 47 mm filter holder, which was to provide the primary means of collection for the inhaled aerosol, along with the various connections that could be manually made to achieve any desired combination of nose and mouth breathing. What cannot be shown are the heating coils located just under the surface of the mannequin—at the front and back torso, in each arm and on the head—to simulate the desired body temperature. Fig. 5b shows the mannequin along with the associated breathing machine (in the suitcase) and the laptop computer that operated and controlled the breathing machine (and heating mechanism) to achieve the desired breathing minute volume, breathing pattern and body temperature. The breathing machine consisted of two pneumatic cylinders—each of volume 1.4 L, for a total of 2.8 L—that could be cycled in and out by a servo-linear actuator. The control system allowed for tidal breathing volumes from 0.1 to 2.5 L (as governed by the distance the pistons traveled), and breathing rate up to 20 breaths min^{-1} (as governed by the speed of travel). Air flowrates were monitored by means of integrated spirometers and body temperatures by means of thermocouples located at strategic locations just under the mannequin surface

Closer inspection of Fig. 5a reveals important specific details of the nose and mouth. During the planned aerosol inhalation experiments, it was an essential feature that the inspired air passed through a filter, which allowed for collection of the inhaled aerosol, and that particles collected on the inner walls of the nose and/or mouth in front of the filter during inspiration should also be recoverable. It was considered especially important that air flowing through the system during the expiration cycle should *not* follow the same route as during inspiration. There was serious concern that particles having been collected on the filter during inspiration, might be reentrained during the expiration part of the cycle, and so exit the mannequin in the exhaled air; and similarly for particulate material collected on the internal walls of the flow system. With these concerns in mind, therefore, the mannequin was designed so that inspired and expired air followed different pathways. This required a complex system of pathways and connectors inside the head, as can be seen in Fig. 5a. But it also required a complex entry and exit system. For nose breathing, this was achieved by allowing air to be inspired through one nostril and out through the other, each measuring 12 mm in diameter, having designed the size of each nostril to be equivalent in area to a pair of nostrils, in order to

ensure approximately the same air velocity at entry and exit. For mouth breathing, the same objective was achieved by providing the mannequin with *two* mouths, each with dimensions equivalent to a 'normal' human mouth, measuring 40 mm in length by 3 mm width, and located immediately adjacent to one another.

For all the experiments, the mannequin was located in the center of the working section of the wind tunnel, connected to a computer that controlled both the heating and breathing parameters through a manifold in the wind tunnel floor. This manifold also contained a mechanism that allowed for rotation of the mannequin about a vertical axis through 360°. For this, the axis of the mannequin was connected to a motor by a belt drive that provided for slow mannequin rotation at about 2 rpm. Since the mannequin had to carry a variety of tubes and wiring that enabled breathing and heated, it was not possible to allow for continuous rotation *in the same direction*. Instead, therefore, the system was set up so that the mannequin could be rotated through the full 360°, at which point a relay was activated such that the direction of rotation was reversed. And similarly after the next 360° of angular travel, and so on and so forth.

During each experiment, the glass fiber filter to be placed in the filter holder was conditioned overnight in a desiccator to stabilize the mass (by reducing the moisture content) then weighed. After sampling the filter was similarly conditioned again, and re-weighed. The difference in the masses provided the mass of particulate material collected on the filter. In addition, the particulate material collected on the inside wall of the tubing between the entry (nose or mouth) and the filter was recovered and weighed. This was done using small cotton balls impregnated with isopropyl alcohol, which were similarly conditioned prior to and after sampling, and again re-weighed at the end. The mass stability of the cotton was shown to be comparable to that for the glass fiber filters when allowed to stabilize in a desiccator for at least 24 hours. The resultant filter and wall particulate masses were combined to provide the total inhaled aerosol mass. From knowledge of the corresponding total volume of air sampled, the aerosol mass concentration was obtained directly.

Reference sampler

An important component in the determination of aspiration efficiency was the measurement of the aerosol reference concentration. Traditionally for aerosol sampling science in wind tunnels, this was carried out using a thin-walled sampler placed facing into the wind and operated isokinetically. That is, the flowrate through the sampler, as generated in this case by a personal sampling pump, was arranged to be such that the average air velocity in the plane of its inlet exactly matched the air velocity in the undisturbed freestream. In this way, it can easily be shown that the aerosol concentration entering the sampler was the same as that in the undisturbed freestream. A great deal has been written about the aspiration efficiency of such a sampler, and the physics is well understood.[1] However, all that is currently known is based on considerations of particle transport in a freestream that is influenced *only* by inertia and *not at all* by gravity. By contrast, in the current scenario of interest, the presence of gravitational effects is the *very* subject of the enquiry. So the possibility of using isokinetic sampling as a reference method at ultralow-windspeeds needs to be approached with caution.

Fortunately, for the special case of isokinetic sampling, where—unlike for less idealized sampling systems—the airflow near the sampler is totally undistorted by the presence and aspirating action of the sampler, its use can be easily justified. A particle travelling towards the sampler inlet follows a trajectory that is influenced both by horizontal convection in the freestream and vertical gravitational settling. So, unlike in the idealized case that has been widely discussed, the particle follows a linear downwards path, the angle of which is determined by the relative speed of convection and gravitational settling respectively. Since the airflow itself is undistorted, then for every particle whose trajectory is taken outside the aspirated air by gravity, it is replaced by another falling into the aspirated air from above. Because the freestream and the aspirated air are perfectly matched, then the particle loss is *exactly* compensated by the particle gain. It follows that isokinetic sampling at ultralow-windspeeds can indeed accurately provide the desired reference concentration. However, because the downwards trajectories of the particles will lead to enhanced deposition on the inside surface of the inlet tube, special care must be taken to recover *all* the aerosol that is aspirated through the plane of the inlet.

For the isokinetic sampling here we used a thin-walled metal probe attached to a 27 mm plastic filter holder, with a plastic cone fitted over the probe to make the sampler more streamlined (thus reducing any significant distortion of the upstream flow). Particulate masses collected on the filter and inside tube wall were obtained in a manner similar to the corresponding ones for the mannequin (as described above). During the aspiration efficiency experiments, the reference sampler was placed upstream of the mannequin in the reference plane and at the same height as the mouth of the mannequin. As suggested earlier, there was a bias between the average concentration in the reference and mannequin planes, respectively. So in the actual experiments, the reference sample values were adjusted to correspond to the mannequin plane using the correction factors shown in Table 4.

Flow visualization

The wind tunnel configuration just described allowed for a desired visualization and recording of the air flow around the mannequin. This work has already been reported separately, and the details are given elsewhere,[14] so will not be repeated in full here. Briefly, the method revolved around a novel smoke tracer technique, in which the smoke itself was generated by incense sticks that were placed in a separate smoke chamber external to the wind tunnel, and then drawn into the tunnel *via* a conduit leading to a tube located vertically in the tunnel upstream of the entrance to the working section. The vertical tube contained small holes drilled along its length into the downstream-facing side such that smoke entering the tube from the generator box was drawn into the tunnel by the negative pressure there. In this way, excellent smoke traces were created that could clearly be seen by the naked eye and easily recorded using a digital camera set up in the mode to record short movie clips from which individual single frames could be extracted for the purpose of presentation.

Aspiration efficiency

For the aspiration efficiency experiments, the mannequin was rotated continuously—albeit reciprocally (as described)—so that, averaged over time, there was no preferred orientation with respect to the wind. During these experiments, aerosol was introduced into the test section of the wind tunnel variously from upstream and above as described earlier. Each sampling run lasted for about 20 min and employed the breathing mannequin, heated to typical skin temperature (33 °C) and dressed in a laboratory coat. The reference sampler was located upstream as already indicated. For the set of experiments presented here, the variables of interest were the windspeed, particle size (MMAD, as measured using the modified Marple personal cascade impactor) and breathing minute volume. A number of individual runs were performed for each set of conditions.

Results

Flow visualization

As already mentioned, a full description of the flow visualization methods has been presented elsewhere, and so too have the results.[14] A short summary is included here for completeness. By way of illustration, Fig. 6 shows an example of the flow visualizations that were recorded, taken from the very large number that encompassed the wide range of conditions of our experiments, and from the many that were presented in our earlier paper. In this particular example, frames from the original movie record were extracted for the peaks of the inspiration and expiration flows, respectively, for mouth breathing only, for the contrasting breathing minute volumes of 6 and 20 L min^{-1}, for windspeed 0.24 m s^{-1}, and for the mannequin facing directly upstream (*i.e.*, no rotation). From these pictures, it can be seen in the first instance that excellent smoke traces were obtained by the method described. Secondly, the effect of the breathing of the mannequin during the expiration phase is very evident. For both minute volumes, the jet of air emanating from the mouth can be clearly seen. Most interestingly, the jet for the higher minute volume is seen to project further into the approaching free-stream, and—even more importantly—persists all the way into the subsequent inspiration phase. Here, therefore, it may be expected that the expiration jet may play a significant role in influencing aerosol spatial and temporal distributions as they relate to inhalability. So the question that was asked in the overall body of the flow visualization work was: over what ranges of conditions of external windspeed, breathing mode and rate, and body temperature does the expiration jet significantly and persistently influence the air movement in the breathing zone of the mannequin, such that it is permanently de-stabilized? For mouth breathing, it was concluded that such de-stabilization occurred under higher breathing rates and at lower windspeeds. Intuitively, this is not surprising. But it had not previously been noted. For nose breathing, the effects were much less, such that de-stabilization occurred only for the highest breathing rate and at the lowest windspeed. Again, this is intuitive since the jet was now projected downwards and not directly out into the freestream. As for body temperature, no influence was found over the full range of conditions studied. Finally, studies at orientations other than forwards-facing showed that all of the aforementioned effects were much reduced or absent. That is, the effects of the breathing of the mannequin were much more in evidence when facing directly upstream.

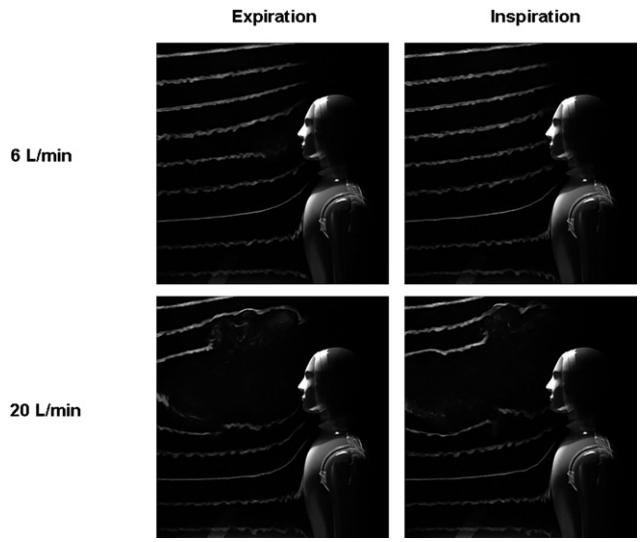

Fig. 6 Examples of flow visualizations in the form of still photographs extracted from the digital movie records, for a windspeed of 0.24 m s^{-1} and mouth-breathing minute volumes of 6 and 20 L min^{-1}.

Aspiration efficiency

Fig. 7 shows some of the preliminary results obtained so far. They are included in this paper to provide an indication of the application of the new experimental system we have described, and will be followed up later by results from the more exhaustive study. Results are shown, from the pre-modified wind tunnel set-up, for the three windspeeds of 0.10, 0.24 and 0.42 m s^{-1} and for mouth breathing mainly at 20 L min^{-1} but

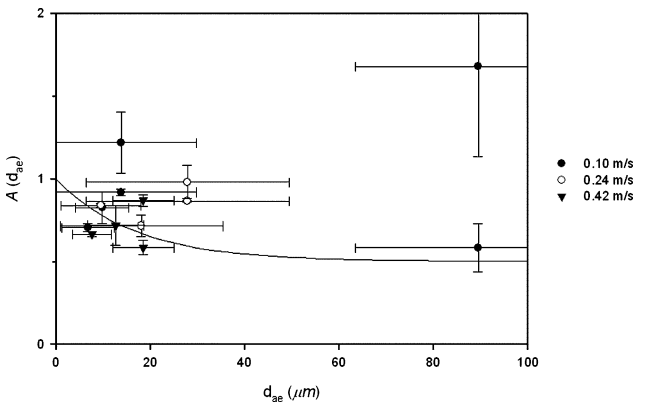

Fig. 7 Early results for the aspiration efficiency of the mannequin as a function of particle aerodynamic diameter, for windspeeds of 0.10, 0.24 and 0.42 m s^{-1} (as indicated), for breathing minute volumes of 6 and 20 L min^{-1}. The horizontal error bars reflect the width of the particle size distribution for the aerosol arriving in the test section and the vertical ones the run-to-run variability (standard error).

with a small number of experiments at 6 L min^{-1}. On this graph, for each data point, the central value on the horizontal axis represents the best estimate of particle size (MMAD) based on the test aerosol characterization described earlier. The error bar represents the geometric standard deviation of the (assumed) log-normal particle size distribution as estimated from the 16% and 84% values. Additionally, for each data point, the central point on the vertical axis represents the average measured value of aspiration efficiency, and the error bar represents the variability as estimated from the multiple runs. On the same graph, for the purpose of comparison with the measured data, is shown the CEN/ISO/ACGIH conventional curve for inhalability. It is too early to start to note any specific trends within the small data set shown so far, except to note that the majority of the results lie close to those obtained previously for faster moving air.

Discussion and conclusions

A new facility has been developed and built in which to study the transport of aerosols at ultralow-windspeeds in the range below 0.5 m s^{-1}, known to be relevant to a large proportion of workplace environments. The facility includes a novel wind tunnel into which well-characterized aerosols, generated from narrowly-graded powders of fused alumina, may be introduced, and a life-size mannequin featuring breathing and body heat. The realization of such a facility was known at the outset to be fraught with considerable experimental difficulties, primarily associated with the introduction and dispersal of aerosols into such a slowly-moving air stream in a manner resulting in a uniform spatial distribution throughout the test section. Although some limitations surfaced, and modifications were made at a number of points during the research so far, a workable system was achieved.

Flow visualization revealed the highly complex nature of the flow near the mannequin during breathing, indicating the importance of the mixing of the jet of expired air with the approaching freestream, and the resultant de-stabilization in the air during inspiration. This was particularly evident at lower windspeeds and higher breathing minute volumes. Such behavior was accurately reflected also in the recent CFD work of Gilmutdinov *et al.*[9] It is expected that the disturbance of the freestream in the breathing zone during aerosol inhalation, containing both random turbulence and coherent flow structures, may well have a strong influence on particle transport to the extent where inhalability itself may be affected. Exactly to what extent is not yet known, based on the relatively small amount of aspiration efficiency data so far, but the knowledge gained from the flow visualization part of the work will be important when we come to interpret the much larger data set that is now emerging.

As for the aspiration efficiency results themselves, it is too early to draw useful conclusions based on the preliminary data set, except to note a few broad features. In general, the results so far are not entirely inconsistent with what has been learned previously from experimental studies at higher windspeeds. That earlier work had shown that the aspiration efficiency of the human head rose sharply at large particles for high windspeeds.[15] According to aerosol sampling theory,[1] aspiration efficiency for a general sampling situation is strongly linked with a number of variables that may be linked through a smaller number of dimensionless groups, including ones representing inertial effects, gravitational effects, orientation effects, sampler shape effects, and relative dimensions (sampler inlet to sampler body size) and—importantly in the present discussion—relative air velocity (windspeed to entry velocity). When the more complete data set is obtained, a closer look at the physics of aerosol aspiration will be useful in interpreting the results, further enlightened by what has been learned about the nature of the flow near the heated, breathing mannequin.

As the work progresses, it will be extended to the study of the sampling efficiencies of a range of personal samplers that will be mounted on the torso of the mannequin, in a manner similar to that during personal sampling of actual workers, as is routinely carried out by professional occupational hygienists. Such measured performances will be compared with the aspiration efficiency of the human head (or some future modified inhalability criterion) for ultralow-windspeeds as determined experimentally during the present body of work.

Acknowledgements

We would like to thank the US-NIOSH for their continued grant support (5-RO1-OH002987-09), Engineering Laboratory Design (Lake City, MN, USA) for its contributions to designing and building the wind tunnel, and Measurement Technology Northwest (Seattle, WA, USA) for its contributions to designing and building the mannequin system.

References

1 J. H. Vincent, *Aerosol Sampling: Science, Standards, Instrumentation and Applications*, Wiley & Sons, Chichester, England UK, 2007.
2 International Standards Organisation (ISO), *Air quality-particle size fraction definitions for health-related sampling*, Technical Report ISO/TR/7708-1983 (E), revised version, ISO, Geneva, Switzerland, 1992.
3 Comité Européen de Normalisation (CEN), *Workplace atmospheres: size fraction definitions for measurement of airborne particles in the workplace*, CEN Standard EN 481, 1992.
4 *Particle Size-Selective Sampling for Particulate Air Contaminants*, ed. J. H. Vincent, American Conference of Governmental Industrial Hygienists, Cincinnati, OH, USA, 1999.
5 R. D. Berry and S. Froude, *An investigation of wind conditions in the workplace to asses their effect on the quantity of dust inhaled, U.K. Health and Safety Executive Report IR/L/DS/89/3*, Health and Safety Executive, London, UK, 1989.
6 P. E. J. Baldwin and A. D. Maynard, A survey of windspeeds in indoor workplaces, *Ann. Occup. Hyg.*, 1998, **20**, 303–313.
7 R. J. Aitken, P. E. J. Baldwin, G. C. Beaumont, L. C. Kenny and A. D. Maynard, Aerosol inhalability in low air movement environments, *J. Aerosol Sci.*, 1999, **30**, 613–626.
8 W. C. Hinds, *Aerosol Technology: Properties, Behavior and Measurement of Airborne Particles*, 2nd edn, Wiley and Sons, New York, 1999.
9 A. Gilmutdinov, I. Zivilskii and S. Zaripov, Three-dimensional modelling of aerosol samplers for unsteady conditions, *J. Environ. Monit.*, 2008, **10**, DOI: 10.1039/b813784f.
10 D. Mark, J. H. Vincent, H. Gibson and W. A. Witherspoon, Applications of closely graded powders of fused alumina as test dusts for aerosol studies, *J. Aerosol Sci.*, 1985, **16**, 125–131.
11 S. Paik and J. H. Vincent, Aspiration efficiency for thin-walled nozzles facing the wind and for very high velocity ratios, *J. Aerosol Sci.*, 2002, **33**, 705–720.

12 W. C. Hinds and T.-L. Kuo, A low-velocity wind tunnel to evaluate inhalability and sampler performance for large dust particles, *Appl. Occup. Environ. Hyg.*, 1995, **10**, 549–556.
13 Y. Wu and J. H. Vincent, A modified Marple-type cascade impactor for assessing particle size distributions in workplaces, *J. Occup. Environ. Hyg.*, 2007, **4**, 798–807.
14 D. K. Schmees, Y.-H. Wu and J. H. Vincent, Visualization of the air flow around a life-sized, heated, breathing mannequin at ultra-low windspeeds, *Ann. Occup. Hyg.*, 2008, DOI: 10.1093/annhyg/men022.
15 J. H. Vincent, D. Mark and B. G. Miller *et al.*, Aerosol inhalability at higher windspeeds, *J. Aerosol Sci.*, 1990, **21**, 577–586.